Black anodic coatings for space applications: study of the process parameters, characteristics and mechanical properties

Yann Goueffon, Laurent Arurault, Catherine Mabru, Claire Tonon, Pascale Guigue

Black anodic coatings for space applications: study of the process parameters, characteristics and mechanical properties

Yann Goueffon[1*], Laurent Arurault[2*], Catherine Mabru[3], Claire Tonon[4], Pascale Guigue[1]

1 CNES, 18 avenue Edouard Belin, 31401 Toulouse Cedex 9, France.

2 Université de Toulouse, CIRIMAT, UPS/INPT/CNRS, LCMIE, Bat 2R1, 118 route de Narbonne, 31062 Toulouse Cedex 9, France.

3 Université de Toulouse, ISAE, Département Mécanique des Structures et Matériaux, 10 avenue Edouard Belin, BP 54032, 31055 Toulouse Cedex 4, France.

4 EADS ASTRIUM Satellites, 31 avenue des Cosmonautes, 31402 Toulouse Cedex 4, France.

* corresponding author :

arurault@chimie.ups-tlse.fr ; phone : 33.561.556.148. ; fax : 33.561.556.163.

Abstract

Black inorganic anodized aluminium alloys are used for managing passive thermal control on spacecraft and for avoiding stray light in optical equipment. Spalling of these coatings has sometimes been observed after thermal cycling on 2XXX and 7XXX aluminium alloys. This phenomenon could generate particulate contamination in satellites and may affect mission lifetime. In this work, the influences of the four main steps of the process (pretreatments, sulphuric anodizing, colouring and sealing) on the coating characteristics have been studied for a 7175 T7351 aluminium alloy. The chemical heterogeneity of the coating has been underlined,

and its mechanical behaviour observed through crazing. Scratch-testing, used to evaluate coating adhesion to its substrate, revealed the negative impact of thermal cycling.

Keywords : aluminium, black anodizing, thermal control, microcracking, optical treatment

1. Introduction

Due to the vacuum of space, thermal regulation of satellites is passively managed by radiative exchange between its external surfaces and the environment. Radiation interactions occur with the Earth, the moon, deep cold space, the sun and the external parts of the satellite. Satellite temperatures in a space environment are often passively controlled by thermo-optical properties of suitable surfaces, ie having convenient solar absorptance (α_s) and emittance (ε). Thus, the utility of black coatings is their α_s/ε ratio close to one, which allows passive thermal control of equipment. Black coatings are also useful to avoid stray light in optical instruments. They can consist of painted surfaces (McCroskey et al., 2000), metal surfaces (Magdy and Ibrahim, 2006), oxide layers obtained by micro-arc oxidation (Shrestha et al., 2006) or anodic films coloured with organic or inorganic dyes (LeVesque et al., 1992; Shih and Huang, 2008]. Black anodic films ($\alpha_s > 0.93$; $\varepsilon_n > 0.90$) including inorganic dyes are mainly used because of their low cost, their corrosive and wear resistances during storage, as well as the low risk of contaminating the spacecraft's instruments, especially by outgassing. The anodic film is grown by electrochemical oxidation of the metal surface, without addition of any substances. From this point of view, the anodic film is not a coating, but a conversion interface tightly bound to the metallic substrate. The adhesion concept is not considered in this case. However in 2005, an alert from the European Space Agency (ESA) (ESA Alert, 2005) mentioned many cases of particle detachment from black anodic films, supported especially on 2XXX and 7XXX type aluminium alloys, after

thermal cycling. Such particle pollution is very hazardous for the lifetime of the satellite, potentially inducing the disturbance of any optical or mechanical mechanisms.

The aim of this research work is to study the operational parameters of the black inorganic anodizing process, especially the pre-treatment steps, and their impact on the anodic film characteristics and properties. Adhesion measurements will be particularly discussed.

2. Experimental procedure

The substrate material was the 7175T7351 aluminium alloy. Its chemical composition in weight percent is: 1.62%Cu, 0.12%Fe, 2.42%Mg, 0.01%Mn, 0.06%Si, 5.75%Zn, 0.041%Ti, 0.21%Cr and Al the remainder. Moreover, all chemical compounds used were analytical grade. Aqueous electrolyte solutions were obtained using deionised water.

2.1 Process of elaboration

The preparation of black anodic films including inorganic dyes followed the ESA Standard (ESA ECSS-Q-70-03A, 2006) for spacecraft design. The process involved four main consecutive steps: surface pretreatments , anodizing, colouring and sealing.

The alloy sheet (3x20x40mm or 10x20x160mm) was degreased with ethanol and then etched in Na_2CO_3 (6.2 g/L) and Na_3PO_4 (12.5 g/L) aqueous mixed solution (pH = 11) for 5 minutes at 93°C and neutralised (this step is often called desmutting) in aqueous HNO_3 (50 %v/v) for 3 minutes at room temperature. The samples were rinsed in distilled water at the end of each step.

The aluminium sheet was then used as anode and a lead plate (3x40x40mm) as counter-electrode in the electrochemical cell. The anodizing was run for 60 minutes in the galvanostatic mode (J_a = 1.2±0.1 A/dm²) using a sulphuric acid solution (150g/L) thermally regulated at 20°C. The samples were then immediately rinsed in distilled water.

The anodized part was coloured by immersion in two successive baths: firstly for 15 min. in a purple solution of cobalt acetate (200g/L) regulated at 43 ±2°C, and then for 10 min in a yellow bath of ammonium hydrosulphide (30g/L) at room temperature. The samples were rinsed in distilled water after each step to remove the excess solution.

The sealing step occurred for 25 minutes in a bath regulated at 98 ±2°C and made up of nickel acetate ($NiCH_3COO$, $4H_2O$) and boric acid (5g/L both).

2.2 Thermal aging

In space, satellites are directly lighted by the sun and then pass into the shadow of Earth, causing thousands of thermal cycles during their lifetime. To simulate the space environment, the ESA Standard (ESA ECSS-Q-70-04A, 1999) recommends performing 100 cycles between -100 and 100°C under vacuum (10^{-5} Pa) with dwells times of 5 minutes minimum and a slope of 10°C per minute. These conditions were defined for the general case and all kinds of materials and equipment (from polymers to electronics). In the current paper, we chose to evaluate the samples, when not otherwise specified, after 10 cycles of -140 to 140°C in a Sun Electronic System EC11 environmental chamber. This could be the maximum range of temperature reached by a satellite orbiting earth. A nitrogen atmosphere was used first to dissociate vacuum and thermal effects. Dwells times of 10 minutes and warming/cooling speeds of 10°C/min were used.

2.3. Microscopic and chemical analysis

The meso- and nanostructures of the coatings were observed by field-emission gun scanning electron microscopy (FEG-SEM) with a JEOL JSM6700F device. Energy Dispersive X-ray (EDX) spectroscopy analyses were performed on the cross-sections of the samples to identify the chemical composition inside the film, and especially the location of the dyes.

The microstructure of the aluminum substrate was observed by optical microscopy after metallographic attack for 30 seconds in an acid bath (1%vol. HF, 1.5% HCl, 2.5% HNO_3 and 95% of distilled water).

2.4 Characterization and mechanical analysis

Surface roughness was measured before and after pretreatment thanks to a perthometer concept using a stylus method. Although the profile of the surface was scanned along a line of 5.6mm, the arithmetic roughness (Ra) was calculated without the first and the last 0.8mm of the profile to avoid edge effects.

Adhesion measurements were evaluated qualitatively using 180° peel tests with tape strengths of 250 and 500g/cm (ESA ECSS-Q-70-13A, 1999) and quantitatively using a scratch-test device (CSM Revetest instrument) with a diamond stylus (Rockwell, 200µm radius tip). Scratch tests were configured with an increasing normal load from 1 to 30N, a loading speed of 30N/min and an advance speed of 5mm/min. The resulting scratch-print of about 5 mm length was then observed by SEM to identify the mechanisms of degradation and to determine the corresponding normal load.

Four-point bending tests were also performed to generate stresses in the coating and then to observe the possible formation and evolution of cracks. Tests were done on a tensile testing device (Adamel DY 26 of 100kN) with a distance between supports of 40mm for the face under compression and 120mm for the face under tension. Samples (10x20x160mm) were observed with the SEM after loading.

3. Results and discussion

The physical and chemical characteristics of the material surface, especially the microstructure and the porosity, were studied during the different steps of the preparation process with a view to explaining the final interface properties.

3.1 Microstructure and porosity

3.1.1. The pre-treatment steps

Fig. 1 shows the initial surface of the AA 7175T7351 just after degreasing and metallographic attack. The grains are long and aligned because of the thermo-mechanical (hot-rolling) processes.

Fig. 1 - Optical microscopic 3D views of the AA 7175T7351 substrate after degreasing and metallographic attack.

Moreover, the aluminium alloy included various irregularly shaped constituent particles, in the range of some microns (Fig. 2a). The EDX analysis revealed that particles contained Al, Fe, Cu, Zn, Mg, in accordance with previous works (Savas and Hearthman, 2008; Gao et al., 1998) that identified for example $Al_{23}CuFe$ phases (Gao et al., 1998) in similar aluminium alloys. The sample showed a metallic appearance, while the arithmetic roughness (R_a) was (0.9±0.1) μm.

The etching in the Na_2CO_3 / Na_3PO_4 aqueous solution blackened the sample. At a mesoscopic scale a tortuous surface appeared (Fig. 2b) with long spots including increasing contents of Zn, Mg and P. The high pH of the etching solution (pH = 11) favours both the chemical dissolution of the "type A" particles (Gao et al., 1998; Buchheit, 1995) and the immediate re-precipitation of their corresponding hydroxides and/or phosphates at the metal surface.

The desmutting step in nitric acid solution dissolved these precipitates at the surface in acidic conditions, leaving a clean surface with abundant irregularly shaped pores a few microns across (Fig. 2c). These pores explain that R_a then increased to (1.8 ±0.1) µm.

3.1.2. The anodizing step

Fig. 2d shows a typical top view of the anodized sample at the mesoscopic scale, while Fig. 3 reports the porosity at higher magnification.

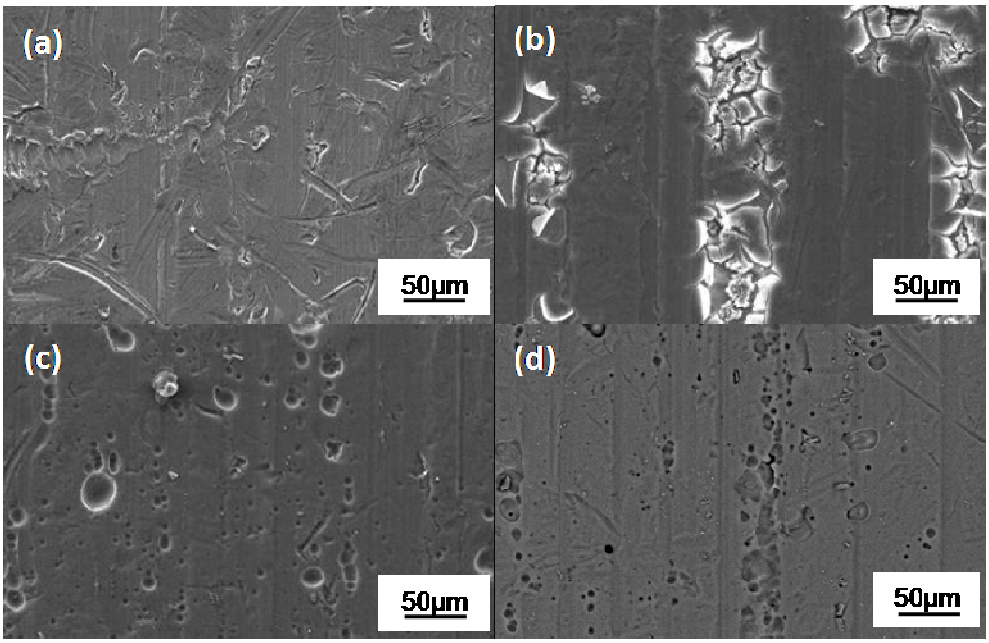

Fig. 2 - SEM plan views of AA 7175T7 at different stages of preparation
(a) after degreasing (b) after etching (c) after deoxidation (d) after anodizing

These results reveal that the first level of porosity, resulting from the chemical dissolution of the microparticles, remained despite the anodizing treatment, which then induced the additional growth of irregular pores varying from about 2 to 100nm.

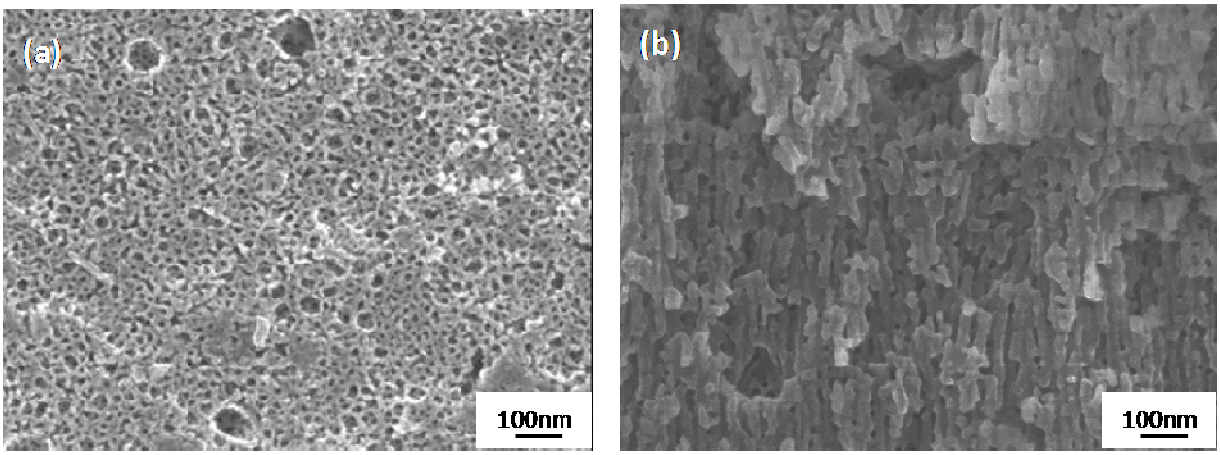

Fig. 3 - FEG-SEM images of the anodic film on the AA 7175T7 just after anodizing
(a) plan view; (b) cross-section view.

The growth of the porous anodic film is usually considered to be a complex process resulting from antagonistic reactions: the electrochemical oxidation of the metal substrate to the Al_2O_3 film, and the chemical dissolution of the anodic layer in highly acidic conditions. The characteristics of the resulting porosity depend on various operational parameters, such as the aluminium alloy used (Konieczny et al., 2004), the experimental anodizing conditions (content, stirring and the bath temperature (Aerts et al., 2007)) and the electrical conditions (Regone et al., 2006). Our results show that the anodic film on AA 7175T7351, includes an erratic spongy structure, clearly different from Keller's long-established model (Keller et al., 1953) made up of regular hexagonal cells, each including a straight central pore perpendicular to the initial substrate surface. This difference is explained by the alloying elements and especially the number and the nature of the constituent microparticles. The usual detailed explanation is based on

changes of local current distributions due to potential differences between the metal matrix and the intermetallic particles.

The thickness of anodic films obtained in sulphuric based electrolytes can vary from 2 to 300µm (Arurault, 2008). In the conditions used here ([H_2SO_4] = 150g/L at 20°C, J_a = 1.2 ±0.1 A/dm² for 60 min.), the resulting thickness was about 20µm, i.e. in accordance with the ESA specification (between 10 and 35µm) for spacecraft design (ESA ECSS-Q-70-03A, 2006).

3.1.3. The sealing step

EDX analysis (Fig. 4) shows the distribution of cobalt, nickel and sulphur in the cross-section of the anodic film of a coloured and sealed sample.

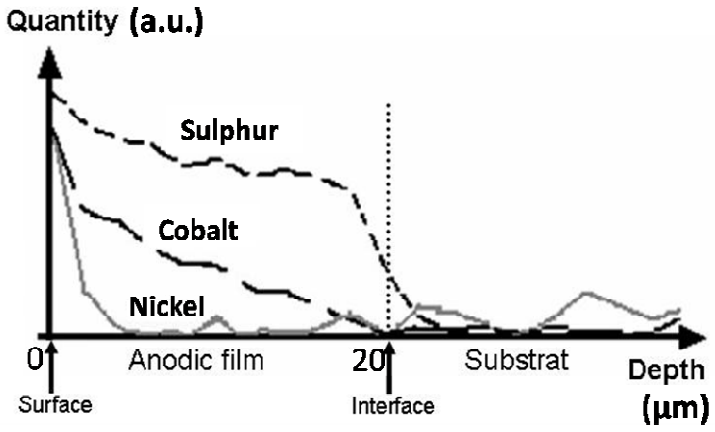

Fig. 4 – EDX analysis of coloured and sealed anodic film on the AA 7175T7351.

Sulphur is present throughout the thickness of the anodic layer, but increases near the film surface and collapses at the interface with the aluminium alloy. The presence of the element sulphur has two possible origins: the first is the introduction of sulphates from the electrolyte ([H_2SO_4] = 150g/L) during anodizing; Thompson (Thompson, 1997) previously indicated that the anodic films obtained in sulphuric based electrolyte have a sulphur content around 12-17 weight%. The second possible origin is the introduction of sulphur during the colouring (second)

step; the increase of sulphur comes from the precipitation of cobalt sulphide taking place inside the pores during the second step of colouring (Sharma et al., 1997) according to:

$$Co(CH_3COO)_2 + (NH_4)_2S \rightarrow CoS + 2\ CH_3COONH_4 \qquad (1)$$

This second origin was confirmed by the presence of cobalt concentrated near the surface (Fig. 4), black CoS being formed in the upper part of the pores due to the immersion colouring process. Nickel was only detected at less than five microns under the surface. This element comes from the sealing bath but its penetration is limited by the presence of CoS particles in the upper part of the pores.

The resulting surface of a coloured and sealed sample was also studied by FEG-SEM at different scales (Fig. 5a and 5b). The plan views reveal no pores on the sample surface but many microcracks at the mesoscopic scale.

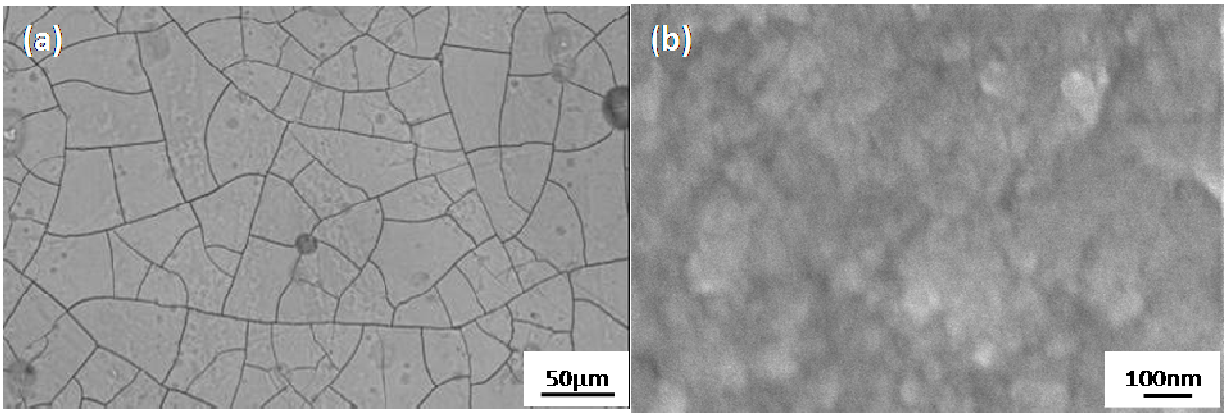

Fig. 5 - FEG-SEM plan views of a coloured and sealed anodic film on the AA 7175T7351 (a) x 200 ; (b) x 60,000.

The mechanism of hydrothermal sealing, usually occurring in pure boiling water, is mainly considered as the hydration of the anodic film, converted into pseudo-boehmite (Alwitt et al., 1992):

$$Al_2O_3 + (n+1)\ H_2O \quad \rightarrow \quad 2AlOOH + n\ H_2O \qquad (n>1) \qquad (2)$$

In this case, the pore closing results from the expansion of the molar volumes, as well as the additional precipitation from the nickel acetate. So, the aim of the sealing step is to close the pores, especially their upper part (Fig. 5a and 5b), to increase efficiency against corrosion and wear resistance, and protect the dyes against the external atmosphere.

But, the main problem remains understanding the origin of the microcracks and their correlation with the mechanical properties in general and with the potential flaking of the final coating in particular.

3.2. Mechanical behaviour

The anodizing process is an electrochemical conversion of the metal surface and does not involve the addition of external material. That is the reason why anodic films are considered sufficiently adherent for the usual applications so the concept of adhesion has not been studied much.

The coloured sealed films were studied from the mechanical point of view, before and after thermal cycling. This cycling simulated the space environment, potentially inducing internal stress, cracking and ultimately flaking of the coatings.

3.2.1. Preparation process, storage and coating stresses

Whatever the process used to prepare the coatings (PVD, CVD...), they usually have residual stresses. For example, Alwitt et al. (Alwitt et al., 1992; Alwitt et al., 1993) showed that, before sealing, non-coloured anodic films on 5657 aluminium alloy anodized in sulphuric acid have tensile stresses around 30 MPa, depending on the substrate and the process parameters, but not on the thickness. However, the sealing step seems to be much more critical because the thermal expansion coefficient is roughly five times greater in the substrate than in the coating (Alwitt et al., 1992). The sealing bath, regulated at 99°C, caused expansion of the aluminium alloy and

subsequent tensile stress in the anodic film. However, once out of the sealing bath, they noted that residual stresses were largely compressive in the sealed films, increasing with sealing time and the thickness of the film.

The influence of humidity on residual stresses of the uncoloured films during long-term exposure to various humidity levels at room temperature were also studied to simulate the effects of space device storage (Alwitt et al., 1992). Aluminium oxide is indeed hygroscopic, and the amount of water adsorbed depends on humidity and temperature. At a level of humidity of 0.02 ppm water, coating stresses are greater than 100MPa tensile while they are between 10 and 30MPa compressive at ambient humidity. On the contrary, a decrease of humidity dehydrates the sealed film, contracting the oxide and inducing tensile stresses. McClung et al. (McClung et al., 1992) particularly noticed that the effects produced by low humidity (0.025ppm) on films grown on the 3XXX and 5XXX series aluminium alloys are reversible and comparable to the effects of a vacuum (10^{-6}Torr).

3.2.2. Cracking

Due to the difference of thermal expansion coefficient between the anodic film and the substrate, heating induces tensile stresses in the coating that can lead to cracking if the fracture limit is reached.

On the anodized 7175 T7351 aluminium alloy, few cracks were observed after the colouring step performed at 43°C. In all the cases, coloured or not, the samples always cracked just after the 99°C sealing step as shown in Fig. 5a. However, on the 5657 aluminium alloy studied by Alwitt et al (Alwitt et al., 1992), no crazing was observed after preparation in spite of high tensile stresses detected during the sealing step. McClung et al. (McClung et al., 1992) studied the

crazing of anodic sulphuric films, sealed but not coloured, on 3XXX and 5XXX series aluminium alloys during heating. They noted that in most cases the first cracks appeared between 100°C and 200°C. But they also noticed that for specimens stored in a damp atmosphere, this critical temperature decreases to around 70°C (Alwitt et al., 1993). In addition, Alwitt et al. (Alwitt and McClung, 1993) found that the crazing temperature depends on the aluminium alloy used, and for a given alloy, on the heat treatment it experienced. Thus, the lower (lower than 100°C) crazing temperature of anodic films produced in sulphuric acid on the 7175 T7351 alloy compared to 3XXX and 5XXX aluminium alloys can be explained. Indeed, alloying elements, and especially copper, change the growth mechanisms of the anodic film; thus the shape of the pores as well as the chemical composition of the anodic films differ from one alloy to another (Garcia-Veraga et al., 2006; Tsangaraki et al., 2006; Liu et al. 2003; Shimizu et al., 1997), changing the mechanical characteristics. For example, the interface between the film and its substrate can be modified by the presence of a layer around 2 nm thick, rich in copper (nearly 40 at. %) (Skeldon et al., 1999). Finally, in the case of coloured films, the dye content of the pores during sealing must also change the thermo-mechanical properties of the anodic film.

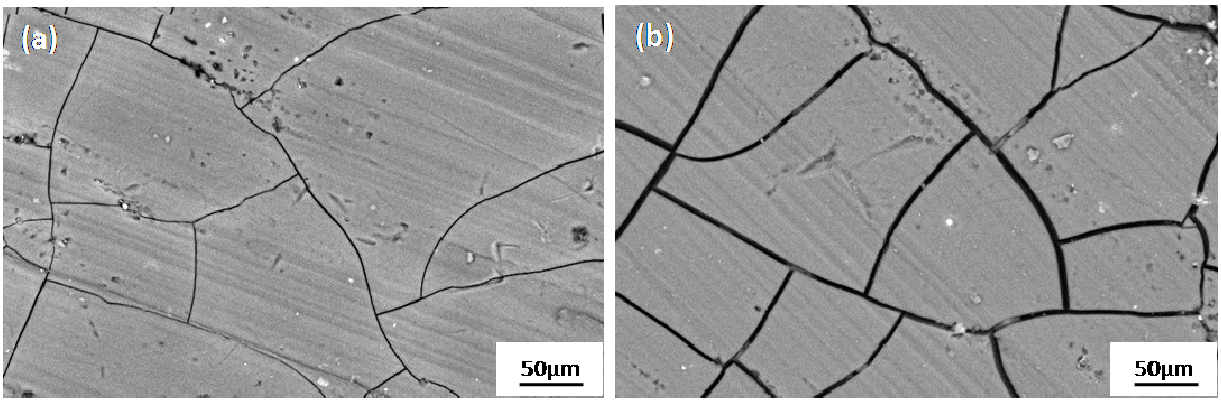

Fig. 6 - SEM plan views of a coloured and sealed anodic film
(a) before thermal cycling (b) after 10 thermal cycles (-140°C/+140°C).

Fig. 6 reveals that thermal cycling (10 cycles between -140°C/+140°C) had no influence on the number of cracks but clearly increased the cracks' width. This can be attributed to a combined effect of dehydration and thermal differential stresses, higher temperatures (compared with the sealing temperature) inducing higher tensile stresses in the anodic film. These results are partially in agreement with similar works (Alwitt et al., 1993) that reported no significant influence of minimal temperature on the crazing while the maximum temperature was found to be highly critical. However, Alwit et al. (Alwitt et al., 1993) showed that the number of cracks always increased as a function of the number of cycles performed on the sample, which is not the case for the present anodized 7175 T7351 aluminium alloy.

The evolution of cracking was observed under mechanical loading, using four-point bending tests to put coatings under both tensile and compressive stresses and to then evaluate adhesion, as done in previous works with other coatings (Richard et al., 1996; Dalmas et al., 2001; Ollendorf and Scheinder, 1999]. SEM observations (Fig. 7a and Fig. 7b) of a strictly identical sample area were performed before and after applying tensile stress. At low loadings (about 2kN), new cracks, mainly perpendicular to the tensile direction of stress, appeared.

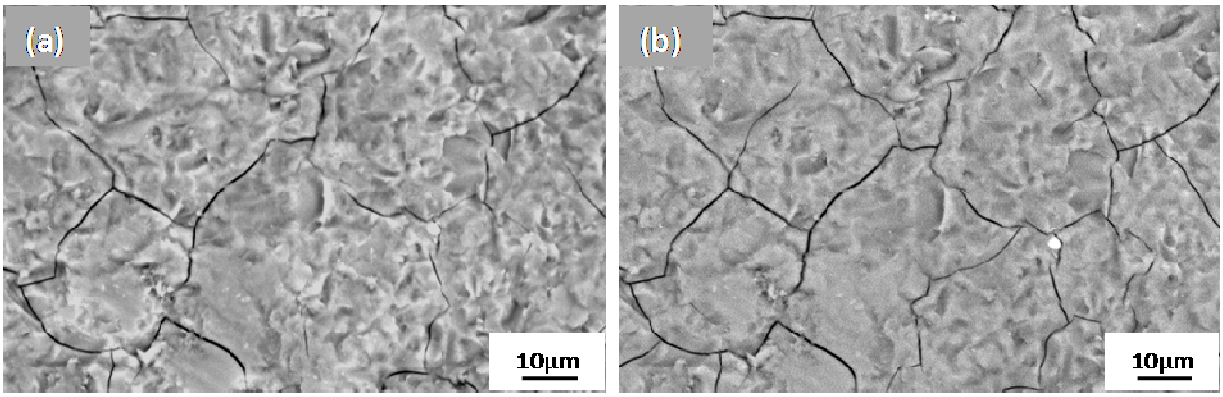

Fig. 7 - SEM plan view of a strictly identical sample area of a coloured and sealed anodic film (a) before four-point bending (b) after four-point bending

The substrate was then under elastic strain. Higher loadings (about 10kN; plastic strain of the substrate) did not cause new cracks. However, it is interesting to note that, during bending, when plastic strains were reached, the face under compressive stress exhibited film flaking whereas the other (under tensile stresses) did not. In particular, this means that compression stresses induced crack propagation along the interface leading to particle detachment, i.e. flaking.

3.2.3. Flaking

The major risk for space applications is not simply the cracking of the surface layer but flaking, because the particles released could settle on cold parts, typically mirrors, lenses or mechanisms. Then the satellite instruments would be damaged decreasing the mission's lifetime. In addition, a high level of flaking could change the thermo-optical properties of the surface affecting thermal control.

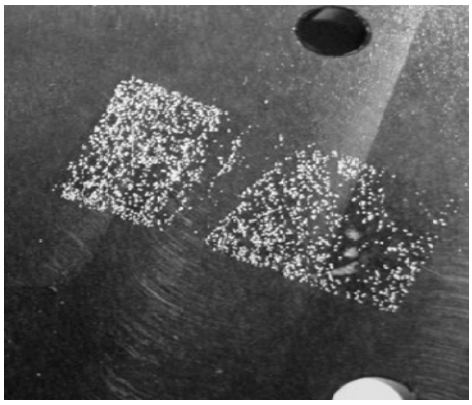

Fig. 8 - Black anodic coating flaked after pulling off a tape for securing a thermocouple

Until now, flaking was always observed on parts that had been thermally cycled. The loss of adhesion was revealed for example on pulling off tapes used to fix thermocouples to the surface during thermal cycles (Fig. 8). However, few cases of self-flaking were observed: particles spontaneously separated from the substrate only under thermal stress. In all cases flaking

occurred on crazed surfaces when the islets delineated by cracks came away. Flaking is thus directly linked to crazing and was previously observed on aluminium alloys especially in the 2XXX and 7XXX series (ESA Alert, 2005).

Peel tests highlighted the influence of thermal cycling on flaking. These tests revealed that black anodized parts, thermally cycled five times between -70 and +100°C, showed a “low removal” of the coating with 250 g/cm tape and “moderate removal” at 500 g/cm. After five cycles between -140°C and +140°C, the removal of the oxide increased at 250 g/cm, while there was complete film removal at 500 g/cm and self-flaking was also observed (without any pulling forces applied). Nevertheless, this test is only qualitative and comparative because the results were strongly dependent on the type of tape used and on the experimental conditions. Thus, other methods to evaluate adhesion quantitatively are necessary.

The scratch test is particularly suited for hard coatings on soft substrates (Darque-Ceretti and Felder, 2003; Bull and Berasetegui, 2006) and is used for instance to study the adhesion of various coatings including TiN (Holmberg et al., 2003) or CN (Liu et al., 2004). Increasing the normal load of the stylus, a critical load can be measured when failure of the coating occurs. Numerous failure modes for thin films are known (Bull, 1997) and models have been developed to calculate adhesion energy thanks to the critical load (Laugier, 1984; Rickerby, 1988). For the present black anodized 7175 T7351 aluminium alloy, scratch tests showed that the critical load was always lower after thermal cycling than before as shown for instance in Fig. 9 (11 and 8 N, before and after thermal cycling, respectively). This therefore provides quantitative confirmation that thermal cycling induces a decrease in the adhesion of the anodic film to the alloy.

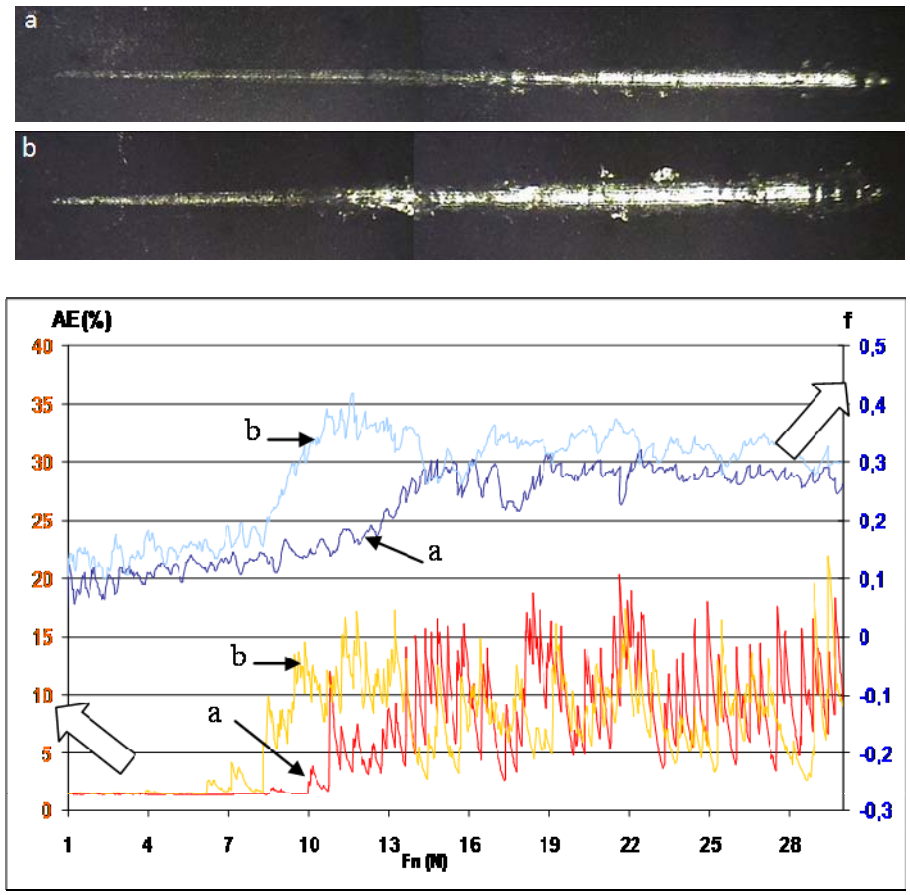

Fig. 9 - Scratch test of a black anodic film followed by SEM (pictures at the top); Acoustic Emission (Left axis) and friction coefficient between stylus and sample (Right Axis) (a) before thermal cycling (b) after 10 thermal cycles (-140°C/+140°C)

Overall, the decrease of adhesion after thermal cycling can be explained by successive tensile and compressive loadings of the coating, mainly due to the difference in thermal expansion between the coating and the substrate. During warming, tensile stresses cause crack propagation across the film and during cooling, compressive stresses result in cracks along the interface, favouring flaking and even self-flaking as observed during four-point bending tests. This mechanism of flaking associated with cooling has already been observed on thermally grown oxides (Chandra et al., 2007; Baleix et al., 2002; Lours et al., 2008).

4. Conclusion

In the current study, we demonstrated that the chemical composition of black inorganic anodic films is heterogeneous, especially due to the colouring and the sealing steps, which only modify the external part of the coating. Nevertheless, on AA 7175 T7351, the coating was spongy throughout its volume due to alloying elements, which modify the mechanical behaviour of the film compared to other AA series. Thermal cycling enlarges cracks and decreases adhesion of the coating according to the scratch-test measurements. Anodic films may crack because of two different phenomena: the difference in the coefficient of thermal expansion between substrate and coating and the drying of the coating.

Further investigations are currently in progress to evaluate the impact of the anodizing and colouring parameters on the characteristics of the film and especially its adhesion. In addition, the roles of humidity and temperature on film cracking during the process and thermal cycling are currently being studied in order to accurately describe the flaking mechanism.

Acknowledgements

The authors thank Peter Winterton for his helpful comments.

References

Aerts, T., Dimogerontakis, Th., De Graeve, I., Fransaer, J., Terryn, H., 2007. Influence of the anodizing temperature on the porosity and the mechanical properties of the porous anodic film. Surf. Coat. Technol. 201, 7310-7317.

Alwitt, R.S., McClung, R.C., 1993. Cracking of anodized coatings on aluminium. Plat. and Surf. Finish. 48-51.

Alwitt, R.S., McClung, R.C., Jacobs, S., 1992. Anodized aluminium coatings for thermal control, Part I: Coating process and stresses. AIAA-922158-CP, In AAIA Technical papers (A92-31285 12-23) Washington, USA, pp. 39-45.

Alwitt, R.S., Xu, J., McClung, R.C., 1993. Stresses in sulphuric acid anodized coatings on aluminium. J. Electrochem. Soc. 140, 5, 1241-1246.

Arurault, L., 2008. Pilling-Bedworth ratio of thick anodic aluminium porous films prepared at high voltages in H_2SO_4 based electrolyte. Trans. Inst. Met. Finish. 86, 1, 51-54.

Baleix, S., Barnhart, G., Lours, P., 2002. Oxidation and oxide spallation of heat resistant cast steels for superplastic forming dies. Mater. Sci. Eng. 327, 155-166.

Buchheit, R.G., 1995. A Compilation of Corrosion Potentials Reported for Intermetallic Phases in Aluminum Alloy. J. Electrochem. Soc.142, 3394-3396.

Bull, S.J., 1997. Failure mode maps in the thin film scratch adhesion test. Tribol. Int. 30, 7, 491-498.

Bull, S.J., Berasetegui, E.G., 2006. Overview of the potential of quantitative coating adhesion measurement by scratch testing. Tribol. Int. 39, 99-114.

Chandra-Ambhorn, S., Wouters, Y., Antoni, L., Toscan, F., Galerie, A., 2007. Adhesion of oxide scales grown on ferritic stainless steels in solid oxide fuel cells temperature and atmosphere conditions. J. Power Sourc. 171, 688–695.

Dalmas, D., Benmedakhene, S., Richard, C., Abdelouahed, L., Béranger, G., Grégoire, T., 2001. Characterization of adherence and cracking within coated materials by an acoustic emission method : application to a WC-Co coating on a steel substrate, Surf. Chem. Catal. 4, 345-350.

Darque-Ceretti, E., Felder, E., 2003. Adhésion – Adhérence. CNRS Editions, Paris, pp 251-264.

ESA Alert, EA-2005-MEP-02-B. PSS-01-703 Inadequate for 2XXX and 7XXX alloys, February 2005. http://alerts.esa.int/

ESA ECSS-Q-70-03A, Black-anodizing of metals with inorganic dyes, April 2006. http://www.ecss.nl (Update of the PSS-01-703)

ESA ECSS-Q-70-04A, Thermal cycling test for the screening of space materials and processes, October 1999. http://www.ecss.nl

ESA ECSS-Q-70-13A, Measurement of the peel and pull-off strength of coatings and finishes using pressure-sensitive tapes, October 1999. http://www.ecss.nl

Gao, M., Feng, C.R., Wei, R.P., 1998. An analytical electron microscopy study of constituent particles in commercial 7075-T6 and 2024-T3 alloys. Metall. Mater. Trans. 29, 4, 1145-1151.

Garcia-Vergara, S.J., El Khazmi, K., Skeldon, P., Thompson, G.E., 2006. Influence of copper on the morphology of porous anodic alumina. Corrosion Sci. 48, 2937-2946.

Holmberg, K., Laukkanen, A., Ronkainen, H., Wallin, K., Varjus, S., 2003. A mode l for stresses, crack generation and fracture toughness calculation in scratched TiN-coated steel surfaces. Wear. 254, 278-291.

Keller, F., Hunter, M.S., Robinson, D.L., 1953. Structural Features of Oxide Coatings on Aluminum. J. Electrochem. Soc. 100, 9, 411-419.

Konieczny, J., Dobrzanski, L.A., Labisz, K., Duszczyk, J., 2004, The influence of cast method and anodizing parameters on structure and layer thickness of aluminium alloys. J. Mater. Process. Tech. 157-158, 718-723.

Laugier, M. T., 1984. An energy approach to the adhesion of coatings using the scratch test. Thin Solid Films. 117, 4, 243-249.

LeVesque, R., Ho, M., Vickers, B., Babel, H., Pard, A., 1992. Black anodize as a thermal control coating for space station freedom. AIAA-92-2160-CP, In AAIA Technical papers (A92-31285 12-23) Washington, USA, pp. 56-65.

Liu, Y., Sultan, E.A., Koroleva, E.V., Skeldon, P., Thompson, G.E., Zhou, X., Shimizu, K., Habazaki, H., 2003. Grain orientation effects on copper enrichment and oxygen generation during anodizing of al-1at.%Cu alloy. Corrosion Sci. 45, 789-797.

Liu, Z., Sun, J., Wu, J.D., Wang, P.N., Shen, W., 2004. Determination of adhesion energy of CNx thin film on silicon from micro-scratch testing. Tribol. Trans. 47, 130-137.

Lours, P., Sniezewski, J., Le Maoult, Y., Pieraggi, B., 2008. Direct observations and analysis of the spallation of alumina scales grown on PM2000 alloy. Mater. Sci. Eng. 480, 40-48.

Magdy, A., Ibrahim, M., 2006. Black nickel electrodeposition from a modified Watts bath. J. Appl. Electrochem. 36, 295-301.

Mc Clung, R.C., Alwitt, R.S., Jacobs, S., 1992. Anodized aluminium coatings for thermal control, Part II: Environmental effects and cracking. AIAA-92-2159-CP, In AAIA Technical papers (A92-31285 12-23) Washington, USA, pp. 46-55.

McCroskey, D.M., Abell, G.C., Chidester, M.H., 2000. Aeroglaze Z306 black paint for cryogenic telescope use: outgassing and water vapor regain. In: SPIE The International Society for Optical Engineering (Ed.) Proceeding SPIE, 4096, pp.119-128.

Ollendorf, H., Schneider, D., 1999. A comparative study of adhesion test methods for hard coatings. Surf. Coat. Technol. 113, 86-102.

Regone, N.N., Freire, C.M.A., Ballester, M., 2006. Al-based anodic films structure observation using field emission gun scanning electron microscopy. J. Mater. Process. Tech. 172, 146-151.

Richard, C.S., Béranger, G., Lu J., Flavenot, J.F., Grégoire, T., 1996. Four-point bending tests of thermally produced Wc-Co coatings. Surf. Coat. Technol. 78, 284-294.

Rickerby, D. S., 1988. A review of the methods for the measurement of coating-substrate adhesion. Surf. Coat. Technol. 36, 1-2, 541-55.

Savas, T.P., Earthman, J.C., 2008. Surface characterization of 7075-T73 aluminium exposed to anodizing pretreatment solutions. J. Mat. Eng. Perform. (under press) DOI: 10.1007/s11665-008-9219-3.

Sharma, A.K., Bhojraj, H., Kaila, V.K., Narayanamurthy, H., 1997. Anodizing and inorganic black coloring of aluminium alloys for space applications. Met. Finish. 95, 12, 14-20.

Shih, H-H., Huang, Y-C., 2008. Study of the black electrolytic coloring of anodized aluminium in cupric sulfate. J. Mater. Process. Tech. (under press) DOI :10 :1016/j.jmatprotec.2007.12.119.

Shimizu, K., Kobayashi, K., Thompson, G.E., Skeldon, P., Wood, G.C., 1997. The influence of θ' precipitates on the anodizing behaviour of binary Al-Cu alloys. Corrosion Sci. 39, 2, 281-284.

Shrestha, S., Shashkov, P., Dunn, B.D., 2006. Microstructural and thermo-optical properties of black Keronite PEO coating on aluminium alloy AA7075 for spacecraft materials applications. In: Proceedings of ISMSE & ICPMSE, SP-616, ESA Publication Division, Collioure, France, pp. s1.5.1-9.

Skeldon, P., Thompson, G.E., Wood, G.C., Zhou, X., Habazaki, H., Shimizu, K., 1999. Interraction of alloying elements during anodizing of dilute Al-Au-Cu and Al-W-Zn alloys and consequences for film growth. Corrosion Sci. 41, 291-304.

Thompson, G.E., 1997. Porous anodic alumina: fabrication, characterization and applications. Thin Solid Films. 297, 1-2, 192-201.

Tsangaraki-Kaplanoglou, I., Theohari, S., Dimogerontakis, Th., Wang, Y.M., Kuo, H.H., Kia, S., 2006. Effect of alloy types on the anodizing process of aluminium. Surf. Coat. Technol. 200, 2634-2641.

Figures Captions

Fig. 1 - Optical microscopic 3D views of the AA 7175T7351 substrate after degreasing and metallographic attack.

Fig. 2 - SEM plan views of AA 7175T7 at different stages of preparation
(a) after degreasing (b) after etching (c) after deoxidation (d) after anodizing

Fig. 3 - FEG-SEM images of the anodic film on the AA 7175T7 just after anodizing
(a) plan view; (b) cross-section view.

Fig. 4 – EDX analysis of coloured and sealed anodic film on the AA 7175T7351.

Fig. 5 - FEG-SEM plan views of a coloured and sealed anodic film on the AA 7175T7351
(a) x 200 ; (b) x 60,000.

Fig. 6 - SEM plan views of a coloured and sealed anodic film
(a) before thermal cycling (b) after 10 thermal cycles (-140°C/+140°C).

Fig. 7 - SEM plan view of a strictly identical sample area of a coloured and sealed anodic film
(a) before four-point bending (b) after four-point bending

Fig. 8 - Black anodic coating flaked after pulling off a tape for securing a thermocouple

Fig. 9 - Scratch test of a black anodic film followed by SEM (pictures at the top); Acoustic Emission (Left axis) and friction coefficient between stylus and sample (Right Axis)
(a) before thermal cycling (b) after 10 thermal cycles (-140°C/+140°C)